Correlation between p53 status, DNA ploidy, proliferation rate and nuclear morphology in breast cancer. An image cytometric study

Katrin Friedrich*, Volker Dimmer, Gunter Haroske, Wolfdietrich Meyer, Franz Theissig and Klaus Dietmar Kunze
Institute of Pathology, Medical Faculty, University of Technology Dresden, Germany

Abstract. The study was designed to detect differences in the nuclear morphology of tumours and tumour cell populations with different p53 expression in correlation with DNA ploidy and proliferation rate. The paraffin sections from routinely processed samples of 88 breast cancers were immunostained with the monoclonal p53-antibody DO-1. After localization and evaluation with a scoring system the sections were destained and stained by the Feulgen method. The nuclei were relocated automatically and measured by means of the image cytometry workstation. Significant differences between the tumours and tumour cell populations with different p53 expression were found in the euploid tumours as well as in the aneuploid tumours and in the breast cancers with a high proliferation rate. The breast cancers with a low immunoreactive score (IRS 1–4) differ from the negative cancers as well as from the cancers with a higher immunoreactive score (IRS 5–12). Evaluating the nuclear populations of the p53 positive cancers, there were differences in the features of the chromatin amount and distribution in the groups of the euploid breast cancers and in cancer with a high proliferation rate. In contrast, the nuclear populations of the aneuploid cancers did not show any differences in their nuclear morphology.

The results showed the different impacts of the p53 expression, DNA ploidy and the proliferation rate on the nuclear morphology in breast cancer.

Keywords: Nuclear morphology, p53 immunohistochemistry, S-phase, G2M-fraction, DNA ploidy

1. Introduction

The wild type of the p53 gene acts as a tumour suppressor gene, which controls the cell cycle at the G1-S-transition. Furthermore, the wild type of p53 can induce apoptosis [3,20,22,23]. Mutations of the p53 gene are a common event in the human carcinogenesis. The mutation of this gene should be associated with a loss of function and also with the loss of the growth suppressor function. Cells with DNA damage remain in the cell cycle, which leads to a higher genetic instability of the tumour.

The genetic instability is often reflected by a DNA aneuploidy. This fact has been confirmed in many studies describing a correlation between the immunohistochemically detected p53 and aneuploidy [4, 7,11]. Some authors also report a higher proliferation rate in p53 positive tumours [1,14,28].

---

*Corresponding author: Katrin Friedrich, Institute of Pathology, Medical Faculty, Technical University Dresden, Fetscherstr. 74, 01307 Dresden, Germany. Tel.: +49 351 4583033; Fax: +49 351 4584358.

The DNA ploidy is only a net estimator of the whole genetic material of the cell populations. Changes in the function of cells like the p53 mutation and the DNA aneuploidy should be associated with changes in the nuclear morphology. These changes may be made objective by high resolution image analysis.

In image cytometric studies, differences in nuclear morphology in correlation with prognostic features were described in breast cancers [2,16,21,23,28,30]. In the past, we reported the correlation of p53 expression and the DNA ploidy as well as differences in the nuclear features in immunohisto-chemically characterized p53 positive and negative breast cancer cells [12,15].

The present study was designed to detect differences in the nuclear morphology in breast cancers as well as nuclear populations being different in their p53 expression in correlation with the DNA ploidy and proliferation. In particular we wanted to know whether differences in the nuclear morphology exist in tumours with a different p53 expression in correlation with the ploidy state and the proliferation rate, respectively. A further question was whether the nuclear populations with a different p53 expression differ in their structure in tumour groups, characterized by the ploidy state and the proliferation rate of the tumours.

2. Material and methods

Forty-nine p53-positive and 39 p53-negative breast cancers were investigated. The tumours were classified according to the WHO nomenclature [19]. The grade of malignancy was determined according to Scarff, Bloom and Richardson [6]. The clinicopathological data of the tumours are detailed in Table 1. The p53 detection was done employing dewaxed paraffin sections of routinely fixed samples. The sections were stained with the monoclonal antibody DO-1 (original supernatant [31], $1:50$ dilution, incubation for 24 h at $4°$C) in an avidin-biotin-peroxidase technique. The chromogen was 3-amino-9-ethylcarbazol (AEC). Finally, the nuclei were counterstained with haemalaun and embedded in glycerol gelatin.

The results of the immunostaining were assessed as an immunoreactive score (IRS) for the whole tumour. The score is the product of the percentage of immunostained cells (divided in 5 groups: 0, 1–10%, 10–50%, 50–80%, 80–100% positive cells) and the staining intensity (weak, moderate and strong reaction). The score ranges from 0 to 12. Breast cancers with a p53 IRS equal one or higher were considered as p53 positive tumours [26].

The image analysis was performed by means of a high resolution image cytometry workstation (Table 2). In each case, 500 nuclei were localized by means of a cytometry workstation. The staining intensity of the nuclei was categorized subjectively in 4 groups: negative nuclei $(-)$, weakly positive nuclei $(+)$, moderately positive nuclei $(++)$ and strongly positive nuclei $(+++)$. After destaining during a 45 min 5N HCl hydrolysis the sections were stained according to the Feulgen method. The actual section thickness was measured by means of the confocal laser scanning microscope LSM-10 (Zeiss, Germany) at three different sites in order to correct some features of the the optical density for sectioning effects. The previously coded nuclei were relocated and measured by means of the cytometry workstation, which consists of an Axioplan microscope (Zeiss, Germany) equipped with a 486/66 MHz IBM compatible PC with a MFG frame grabber (Imaging Technology, USA) using a CCD TV camera XC-77 CE (Sony, Japan) and a computer controlled motor driven xy-scanning stage. The software based on the OPTIMAS image analysis system (OPTIMAS Corp., Seattle, WA, USA). Correction procedures for the section thickness, diffraction and glare were implemented in the software [17]. From each nucleus, 97 nuclear features derived from the segmented extinction image

Table 1
Clinical data

	p53 positive cases	p53 negative cases
Tumour size		
pT1	20	18
pT2	27	18
pT3	1	1
pT4	1	1
pTx	0	1
Lymph node status		
pN0	23	19
pN1	20	17
pN2	1	0
pNx	5	3
Bloom–Richardson-grading		
G1	3	8
G2	18	19
G3	28	12
Age	58.5 (range 27–87)	59 (range 36–83)
DNA-ploidy		
Peridiploid	3	9
Peritetraploid	21	11
Aneuploid	25	19
S-phase		
lower or equal 5%	21	21
higher than 5%	27	17
not estimated	1	1
G2M-fraction		
lower or equal 5%	20	18
higher than 5%	28	20
not estimated	1	1

Table 2
Technical equipment for the image cytometry system

Instrument	Specification	Source
Microscope	Axioplan®	Zeiss
Light source	Halogen lamp 12 V, 100W	Zeiss
Power supply	not specified	Zeiss
Filter	Interference filter 570 nm	Zeiss
Condensor	Condensor 0.9	Zeiss
Objective	Plan NEOFLUAR $\times$ 63/1.25 oil	Zeiss
xy-scanning stage	with MCU 26	Zeiss
Adapter	C-mount without optical lenses	Zeiss
TV camera	XC77CE pixel size: 11×11 μm; 0.03 μm^2 in the object plane	Sony
Frame grabber	MFG	Imaging Technology
Image analysis basic software	Optimas®	OPTIMAS

were computed on a MicroVAX 4000 computer (DEC, Maynard, MA, USA) which is connected via Ethernet to the image analysis workstation. The nuclear features describe the size and shape of the nucleus, the amount, the statistical and topological distribution of the chromatin and chromatin statistics in the "flat image" (Table 3).

Table 3
Acronyms of the cytometric features

Acronym	Short description
Features describing the nuclear shape and size	
FormFak	Shape factor of the nucleus
VarKRad	Variation coefficient of the contour radii of the nucleus
Res02	Contour difference to a fitted ellipse
RVKont	Radius ratio of the nuclear contour
RVKonv	Radius ratio of the nuclear convex contour
KonvVerh	Ratio of the area and the convex contour area
KontFl	Area of the nucleus
KonvFl	Convex contour area
FFKonv	Shape factor of the convex contour
Loch	Relative proportion of nuclear holes
ZEIKOFl	Area according line coincidence
Features describing the chromatin amount	
IODnc	Integrated optical density without correction for section thickness
IOD	Integrated optical density with stereological correction of section thickness
Features describing the chromatin distribution	
nGran	Number of coarse chromatin particles
MaxTextK	Number of relative maxima of the texture curve
RIODHet	Percentage of heterochromatin optical density and nuclear IOD
SKEWExt	Skewness of the optical density histogram of the nucleus
FS1M	Mean extinction of the "flat image" (first moment of fine structure)
FS2M	Standard deviation of the extinction of the flat image (second moment of fine structure)
FS3M	Skewness of the extinction of the flat image (third moment of fine structure)
GT2sig	Number of objects darker than $2 \times SD$ of the flat image extinction
LT2sig	Number of objects brighter than $2 \times SD$ of the flat image extinction
MOD	Optical density in the median filtered image
RadExt	Relative mean radial extinction distribution
RadSTD	Relative standard deviation of the radial extinction
AziSTD	Relative standard deviation of the azimutal extinction
AziDiff	Relative maximal azimutal extinction difference
NucZahl	"Number of nucleoli"
InvMo	52 invariant moments of the heterochromatin topology according to Hu
Node	Number of nodes in the texture tree
Width	Width of the texture tree
Features describing the chromatin distribution in a median filtered image	
FnGran-FLT2sig	Features nGran-LT2sig in a median filtered image
FSTDObj	Standard deviation of the optical density histogram of the nucleus
FExtObj	Extinction range of all object thresholds
FExtGran	Mean extinction of the coarse chromatin particles
FExtBas	Extinction range of the lowest possible segmentation threshold
FExtHet	Mean extinction of the heterochromatin

The DNA image cytometry was performed on fine needle aspirates or imprints from fresh tumour material which were stained according to the Feulgen method. The DNA ploidy was assessed by the cytometry workstation. In each case at least 250 tumour cell nuclei and 20–30 lymphocytes as internal reference cells were measured. The DNA ploidy status of the tumours was classified as peridiploid, peritetraploid and aneuploid.

For the flow cytometry, samples of fine needle aspirates from fresh tumour material were used for the estimation of S-Phase and G2/M-fraction by the FACScan (Becton/Dickinson) with the test kit Cycle test.

For the univariate and multivariate statistical analyses which are based on the mean values and their standard deviations of the features from the nuclear populations in each staining category for each case, a self written software program REDUGD was used. The Bonferroni principle was applied for defining significance levels at $p < 0.05$ in the multivariate analyses. According to this principle the significance level desired for the actual discrimination ($p < 0.05$) has to be divided by the appropriate degree of freedom (equal the number of the uncorrelated variables).

3. Results

3.1. Comparison of the whole nuclear populations from tumours with different p53 IRS in groups startified by their DNA ploidy and their proliferation rate

In this section, only the immunoreactive score of the whole nuclear population will be taken into consideration.

Differences between differently scored breast cancers were found in the euploid and aneuploid tumour groups. Whereas the peridiploid and peritetraploid tumours showed a higher irregularity of the chromatin distribution in the p53 positive tumours, the aneuploid cancers showed a higher degree of polymorphism in the tumours with a positive p53 reaction than their negative counterparts (Table 4).

When the whole nuclear population of the p53 positive tumours was evaluated, there was a difference between the peridiploid and the peritetraploid cancers in a feature of the chromatin distribution (SD FExtBas; higher in the tetraploid cancers). However, the p53 positive nuclei of the peritetraploid cancers showed the higher values in a feature of the nuclear size, in the number of the coarse chromatin particles and in the standard deviation of two invariant moments of the chromatin structure than the diploid cancers (Table 5).

In the p53 negative tumours, the group of the diploid and tetraploid cancers differs from the aneuploid tumours in a feature, describing a higher variability of the elliptical shape in the aneuploid tumours.

In breast cancers with a high proliferation rate (S-Phase and G2M fraction greater than 5%, respectively), a number of significant different features were found. They describe a higher degree of polymorphism of the nuclei in the p53 positive tumours compared with the cancers without immuno-histochemically detectable p53. Furthermore, the p53 positive tumours also had nuclei with irregular chromatin distribution and a variable amount of chromatin (Tables 6, 7).

Table 4

Significantly different features in euploid (di- and tetraploid) and aneuploid tumours with different p53 expression ($p < 0.05$)

Feature	p53 negative	IRS 1–4	IRS 5–12
Euploid tumours			
SD percentage of heterochromatin optical density and nuclear IOD*	0.173	0.231	0.202
SD 3rd moment of fine structure	0.946	1.271	1.123
invariant moment 22	0.501×10^{-4}	0.439×10^{-4}	0.156×10^{-3}
Aneuploid tumours			
SD integrated optical density (without correction of section thickness)	7305	8018	12411
SD ration of the area and the convex contour area*	0.014	0.018	0.019
SD invariant moment 11*	0.406×10^{-2}	0.254×10^{-2}	0.394×10^{-2}

SD ... standard deviation; p53 negative ... p53 negative tumours; IRS 1–4 ... weakly positive tumours;
IRS 5–12 ... strongly positive tumours; IRS ... immunoreactive score.
*Best combination of features with significant difference in the multivariate analysis.

Table 5

Significant different features in p53 positive nuclei of the diploid and tetraploid tumours ($p < 0.05$)

Feature	Diploid	Tetraploid tumours
SD skewness of the optical density histogram of the nucleus in a median filtered image	0.475	0.382
Area according line coincidence*	1735	2351
Number of coarse chromatin particles*	5.256	6.424
SD invariant moment 4*	0.476×10^{-6}	0.485×10^{-6}
SD invariant moment 6*	0.476×10^{-6}	0.485×10^{-6}

*Best combination of features with significant difference in the multivariate analysis.

Table 6

Significance in different features of tumours with different p53 expression with a S-phase greater than 5% ($p < 0.05$)

Feature	p53 negative	IRS 1–4	IRS 5–12
SD integrated optical density (without correction of section thickness)*	7699	8876	14431
SD area according line coincidence	539	707	815
Second moment of fine structure	0.042	0.031	0.032
SD area of the nucleus	574	737	854
SD convex contour area	605	776	893
SD relative standard deviation of the radial extinction	0.032	0.027	0.032
SD Standard deviation of the optical density histogram of the nucleus	2.804	2.128	2.601

SD ... standard deviation; p53 negative ... p53 negative tumours; IRS 1–4 ... weakly positive tumours; IRS 5–12 ... strongly positive tumours; IRS ... immunoreactive score.
*Best combination of features with significant difference in the multivariate analysis.

Table 7

Significance in different features of tumours with different p53 expression with a G2M-fraction greater than 5% ($p < 0.05$)

Feature	p53 negative	IRS 1–4	IRS 5–12
SD area according line coincidence*	467	680	778
SD area of the nucleus	492	719	824
SD convex contour area	516	756	864
SD contour difference to a fitted ellipse	0.478	0.535	0.649
SD integrated optical density (without correction for section thickness)	6864	7649	12980
SD ratio of the area and the convex contour area	0.014	0.018	0.019
Contour difference to a fitted ellipse	1.234	1.495	1.680
SD number of coarse chromatin particles	10.270	14.950	14.950
SD number of nodes in the texture tree	5.056	6.827	7.373
SD shape factor of the nucleus	1.800	2.237	2.235
SD number of coarse chromatin particles in a median filtered image	5.093	6.888	7.451
SD "number of nuclei"	8.390	11.190	12.070
SD number of objects darker than $2 \times$ SD of the flat image extinction in a median filtered image	5.445	6.548	7.267
SD integrated optical density (with correction of section thickness)	15773	16357	28615
SD invariant moment 3	0.210×10^{-3}	0.205×10^{-3}	0.341×10^{-3}
SD width of the texture tree	2.583	3.261	3.471
SD invariant moment 13	0.791×10^{-4}	0.566×10^{-4}	0.210×10^{-3}
SD percentage of heterochromatin optical density and nuclear IOD	0.170	0.229	0.214
Invariant moment 12	0.262×10^{-4}	0.226×10^{-4}	0.543×10^{-3}

SD ... standard deviation; p53 negative ... p53 negative tumours; IRS 1–4 ... weakly positive tumours; IRS 5–12 ... strongly positive tumours; IRS ... immunoreactive score.
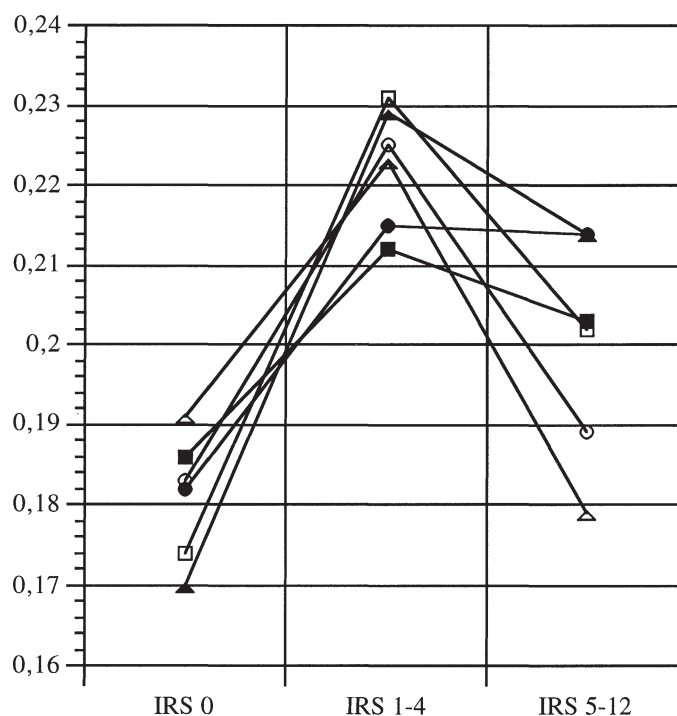*Best combination of features with significant difference in the multivariate analysis.

Fig. 1. Standard deviation of the percentage of heterochromatin optical density in the nuclear integrated optical density in breast cancers with different p53 expression in correlation to DNA ploidy, S-phase and G2M-fraction. IRS 0 . . . p53 negative tumours; IRS 1–4 . . . weakly p53 positive tumours; IRS 5–12 . . . strongly positive tumours. □ peri-, di- and tetraploid; ■ aneuploid; ○ S-phase < 5%; ● S-phase > 5%; △ G2M-fraction < 5%; ▲ G2M-fraction > 5%.

As shown in Tables 4–6 and in Figs 1 and 2, the breast cancers with an IRS 1–4 differ from the negative as well as from the more strongly positive tumours (IRS 5–12) in some features of chromatin amount and distribution.

3.2. Comparison of nuclear subpopulations with different p53 expression in groups stratified by their DNA ploidy and their proliferation rate

The nuclear populations differ in their morphology concerning to the p53 expression in the group of peridiploid and peritetraploid tumours and in tumours with a S-phase and G2M fraction higher than 5%, respectively.

The peridiploid and peritetraploid tumours were different in some features of the chromatin distribution and amount. In general, the texture of the nucleus seems to be more homogeneous in the p53 positive population than in the negative nuclei. The mean values of some optical density features were lower in the more strongly p53 positive nuclei. On the other hand, the standard deviation of the integrated optical density increased with the p53 stainability. In the multivariate analysis, the skewness of the optical density was the feature with a significant difference (Table 8; Figs 3, 4).

Breast cancers with a S-phase fraction higher than 5% showed differences in features for the distribution and amount of chromatin, as well. The best discriminant features in the multivariate analyses were the percentage of the heterochromatin optical density of the heterochromatin in the integrated optical density of the whole nucleus and the standard deviation of the integrated optical density.
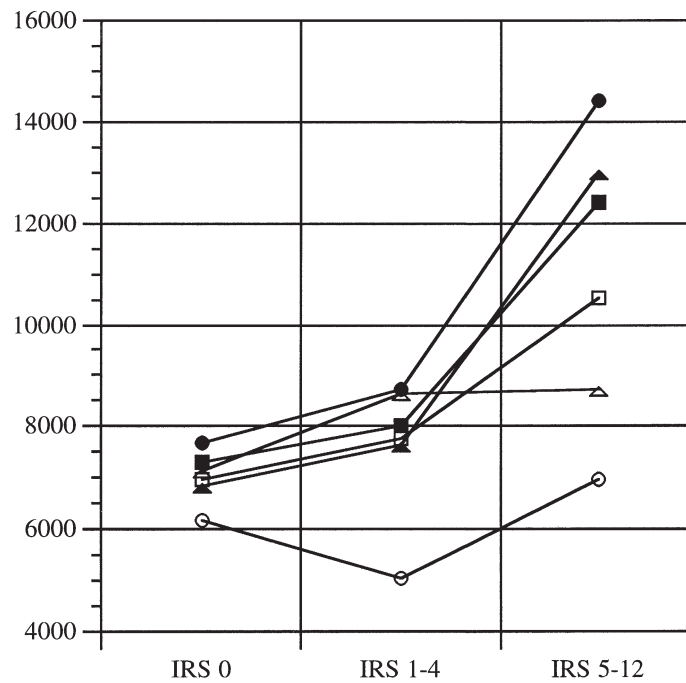
Fig. 2. Standard deviation of the integrated optical density in breast cancers with different p53 expression in correlation to DNA ploidy, S-phase and G2M-fraction. IRS 0... p53 negative tumours; IRS 1–4... weakly p53 positive tumours; IRS 5–12... strongly positive tumours. □ peri-, di- and tetraploid; ■ aneuploid; ○ S-phase $< 5\%$; ● S-phase $> 5\%$; △ G2M-fraction $< 5\%$; ▲ G2M-fraction $> 5\%$.

Table 8

Significant differences in the nuclear subpopulations with different p53 expression in the euploid (di- and tetraploid) p53 positive tumours ($p < 0.05$)

Feature	p53−	p53+	p53++	p53+++
Skewness of the optical density histogram of the nucleus[*]	0.520	0.432	0.311	0.090
Skewness of the optical density histogram of the nucleus in a median filtered image	0.456	0.373	0.258	0.0335
Percentage of heterochromatin optical density in the nuclear IOD	0.366	0.401	0.438	0.537
SD integrated optical density (without correction of section thickness)	6764	8891	9762	12817
Extinction range of all object thresholds in a median filtered image	1.859	1.798	1.728	1.579
Mean extinction of the coarse chromatin particles in a median filtered image	1.290	1.272	1.260	1.234
Mean extinction of the heterochromatin	1.374	1.330	1.288	1.192

SD... standard deviation; p53−... p53 negative nuclei; p53+... weakly p53 positive nuclei;
p53++... moderately p53 positive nuclei; p53+++... strongly p53 positive nuclei.
[*]Best combination of features with significant difference in the multivariate analysis.

When the cancers with a high G2M-fraction (higher than 5%) were taken into consideration, many features showed significant differences in the univariate analysis. In these tumours, the irregularity of the nuclear shape increases and correlates with the p53 expression. However, the multivariate analysis resulted in significant differences in two features describing the amount and distribution of chromatin (Table 9; Figs 3, 4).
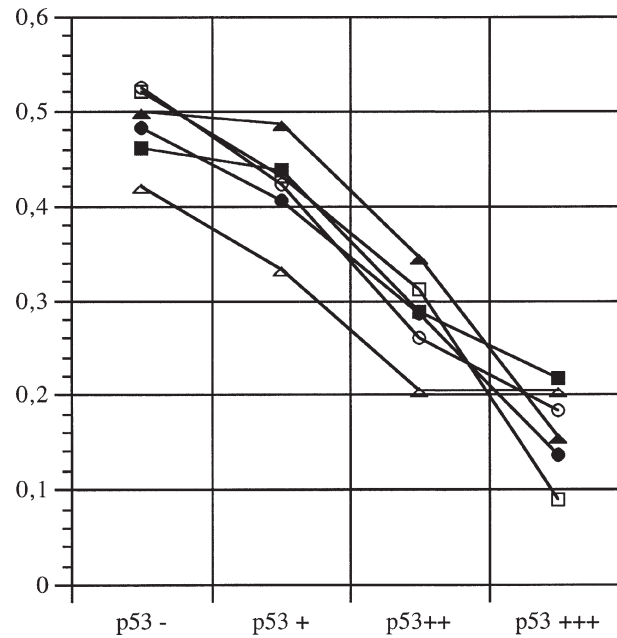
Fig. 3. Skewness of the optical density histogram of the nucleus in nuclear subpopulations with different p53 expression in correlation to DNA ploidy, S-phase and G2M-fraction. p53− . . . p53 negative nuclei; p53+ . . . weakly p53 positive nuclei; p53+ + . . . moderatly p53 positive nuclei; p53+ + + . . . strongly positive nuclei. □ peri-, di- and tetraploid; ■ aneuploid; ○ S-phase < 5%; ● S-phase > 5%; △ G2M-fraction < 5%; ▲ G2M-fraction > 5%.
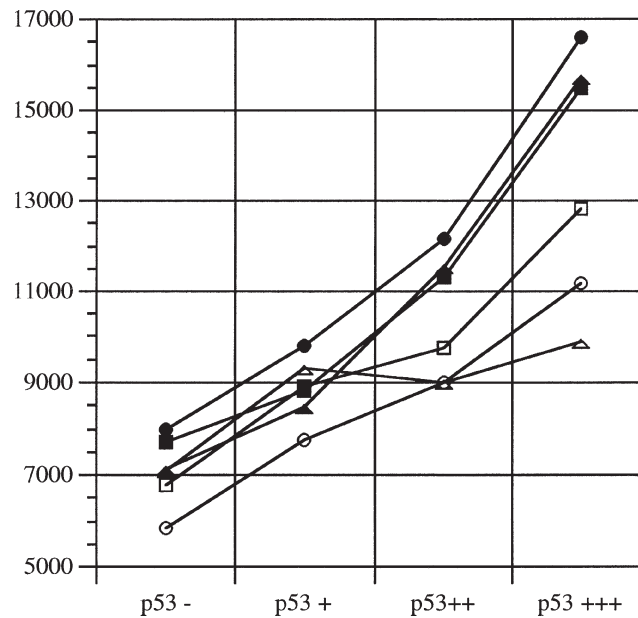

Fig. 4. Standard deviation of integrated optical density in nuclear subpopulations with different p53 expression in correlation to DNA ploidy, S-phase and G2M-fraction. p53− . . . p53 negative nuclei; p53+ . . . weakly p53 positive nuclei; p53+ + . . . moderatly p53 positive nuclei; p53+ + + . . . strongly positive nuclei. □ peri-, di- and tetraploid; ■ aneuploid; ○ S-phase < 5%; ● S-phase > 5%; △ G2M-fraction < 5%; ▲ G2M-fraction > 5%.

Table 9
Significant differences in the nuclear subpopulations with different p53 expression in the p53 positive tumours with a S-phase and a G2M-fraction higher than 5% ($p < 0.05$)

Feature	p53−	p53+	p53++	p53+++
S-phase > 5%				
SD integrated optical density (without correction of section thickness)*	7996	9783	12143	16590
Skewness of the optical density histogram of the nucleus*	0.483	0.405	0.287	0.137
Skewness of the optical density histogram of the nucleus in a median filtered image*	0.425	0.352	0.234	0.080
SD integrated optical density (with correction of section thickness)	18162	22103	25485	37368
Extinction range of all object thresholds in a median filtered image	1.852	1.799	1.730	1.610
Second moment of fine structure in a median filtered image	0.242	0.237	0.205	0.168
Percentage of heterochromatin optical density and nuclear IOD	0.374	0.414	0.450	0.520
Mean extinction of the heterochromatin in a median filtered image	1.369	1.333	1.287	1.209
Third moment of fine structure	−0.412	−0.492	−0.265	0.535
G2M-fraction > 5%				
SD integrated optical density (without correction of section thickness)*	7123	8446	1155	15715
SD integrated optical density (with correction of section thickness)	15644	18204	24316	35378
Skewness of the optical density histogram of the nucleus	0.499	0.486	0.346	0.156
Skewness of the optical density histogram of the nucleus in a median filtered image	0.435	0.435	0.293	0.100
SD area according line coincidence	543	631	734	815
Second moment of fine structure in a median filtered image	0.250	0.255	0.218	0.174
Integrated optical density (without correction of section thickness)	26835	29761	34112	40617
Extinction range of all object thresholds in a median filtered image*	1.834	1.851	1.760	1.616
Third moment of fine structure in a median filtered image	0.276	0.114	0.379	1.025
Contour difference to a fitted ellipse	1.360	1.655	1.661	1.658
Third moment of fine structure	−0.381	−0.642	−0.413	0.396
Percentage of heterochromatin optical density and nuclear IOD	0.381	0.390	0.428	0.515
Shape factor of the convex contour	13.760	13.830	14.060	14.280
Radius ratio of the nuclear convex contour	0.719	0.713	0.684	0.660
Variation coefficient of the contour radii of the nucleus	0.135	0.1408	0.155	0.168
SD contour difference to a fitted ellipse	0.514	0.568	0.621	0.683
Mean extinction of the heterochromatin in a median filtered image	1.356	1.369	1.306	1.212
Extinction range of the lowest possible segmentation threshold	0.682	0.644	0.684	0.757

SD ... standard deviation; p53− ... p53 negative nuclei; p53+ ... weakly p53 positive nuclei;
p53+ + ... moderately p53 positive nuclei; p53+ + + ... strongly p53 positive nuclei.
*Best combination of features with significant difference in the multivariate analysis.

4. Discussion

The differences between differently scored tumours were found in tumours with a high proliferation rate and in the groups of euploid and aneuploid breast cancers. The aneuploid cancers as well as the subgroups with a high proliferation rate showed an increase of nuclear polymorphism with the p53 immunoreactive score. Moreover, the aneuploid stronger p53 positive breast cancers also show a higher degree of polychromasia than their p53 negative counterparts. An exception in this part of the study are the peridiploid and peritetraploid tumours which differ only in chromatin distribution features.

The association between the p53 immunostaining and aneuploidy is a well-known fact. A significant relationship between p53 expression and aneuploidy was confirmed in a previous study on breast cancers [11]. Remivikos et al. [27] also found an association between the ploidy state and the p53 expression in cell population in a flow cytometric study of colorectal carcinomas.

Falkmer et al. [9,10] reported different ploidy states in cells of neuroendocrine tumours using a methodological approach similar to the present study.

Other reports describe a correlation between the p53 immunostainability and the S-phase/G2M-fraction in flow cytometric studies [25]. However, we did not find a significant correlation between the p53 expression and the S-phase or G2M fraction in the present study. One possible reason may be the selection of the cases by their p53 status and not by a random or consecutive sampling as in the above mentioned studies.

In all groups with significant differences in the nuclear morphology, the breast cancers with an IRS 1–4 are distinguished from the negative and the more strongly positive (IRS 5–12) tumours in some features describing the chromatin distribution. These findings may suggest a different significance of the immunohistochemical detectable p53 protein [5]. The antibody DO-1 used here recognizes an epitope that is present on both the mutated and on the wild type p53 protein [31]. In another study [18], which includes some cases found in the present one, the p53 gene was found mutated only in tumours with a high IRS percentage of p53 positive cells by means of the PCR analysis. In the tumours with an IRS 1–4/low percentage of positive cells, the immunohistochemically detected protein may correspond to the wild type of the p53 protein with a prolonged life span. This may be the result of a binding of the p53 protein to other molecules. Another possible interpretation of this phenomenon is an increased expression of the wild type protein caused by a DNA damage. Changes in DNA are a common event in malignomas, but it is not known whether such DNA damage during the malignant transformation and progression may lead to an induction of the p53 wild type expression.

Taking into consideration the different nuclear populations of the p53 positive tumours, it becomes evident that only nuclei from diploid and tetraploid tumours show differences in correlation with the p53 expression in their nuclear features, but not the nuclei of aneuploid tumours. The higher degree of dedifferentiation in aneuploid tumours could be one reason for the missing correlation in p53 expression and the nuclear features in these tumours. This agrees with some findings of a previous study, which examined the morphological nuclear features in correlation with the p53 expression in breast cancer with different stages of the tumour disease, reflected by the clinicopathological features. In this study we found a higher influence of the immunohistochemical detected p53 on the nuclear morphology in cancers in early stage of disease than in those in a more advanced stage [13].

In detail, the nuclei of the peridiploid and peritetraploid tumours with a higher p53 immunoreactivity showed a more homogeneous nuclear texture than their negative counterparts. The mean values for some optical density features decrease with respect to the p53 expression, i.e., the nuclei in the p53 positive populations are paler than the p53 negative cells. In general, the transcriptionally active chromatin is characterized by a lower stainability than the inactive heterochromatin. The paleness of the nuclei in the p53 positive populations may suggest a higher rate of transcription in these cells. The stronger p53 positive nuclear populations showed a greater variability in the chromatin amount than the p53 negative nuclei in these euploid cancers. This observation agrees with the well-known phenomenon of polychromasia. On the other hand, it appears to be contradictory to the non-aneuploid state of these tumours. This group includes tumours with diploid or tetraploid nuclei, as well as tumours with a mixed diploid and tetraploid nuclear population. The chromatin amount reflected by the integrated optical density should also be different in these non-aneuploid tumours.

The whole nuclear population (including the p53 positive and the p53 negative nuclei) of the p53 positive tumours showed a difference between the diploid and the tetraploid cancers only in a feature of the chromatin distribution. In contrast, the p53 positive nuclei of these cases were different in their chromatin distribution as well as in their nuclear size, whereas in the negative nuclear population of the p53 positive cancers no difference could be found in the nuclear features. This may suggest a stronger impact of the p53 positive cell population on the nuclear morphology in both of these ploidy groups.

Significant differences in the nuclear morphology correlated with the p53 expression could be found only in tumours with a high proliferation rate, but not in those with a low proliferation rate. This seems to be in contradiction to the above mentioned differences in the diploid and tetraploid tumour group and the results of a previous study which describes a higher degree of association between the p53 expression and nuclear morphology in breast cancers with favorable prognostic criteria than in those with an unfavorable prognosis. A high rate of proliferation in breast cancers is also a sign of an unfavorable prognosis, but this is not the same as aneuploidy.

The changes in the nuclear populations of tumours with a high proliferation rate with different p53 expression are the same as those in the group of the euploid tumours. Additionally, the p53 positive population in tumours with a G2M-fraction higher than 5% exhibit a more irregular shape than the negative or lower p53 positive nuclei. The loss of p53 function in cells with mutated p53 protein should result in a higher proliferation rate of this cell population. The S-phase and the G2M-phase are also associated with changes in the morphology of the nucleus. The p53 associated changes in nuclear morphology cannot be separated from this proliferation associated nuclear pattern.

In conclusion, the results show the different impact of the p53 state on the one hand, and the DNA ploidy and the proliferation on the nuclear morphology on the other. Furthermore, there are hints for a different impact of subpopulations with a different p53 expression for the nuclear morphology especially in the euploid breast cancers.

Acknowledgements

References

[1] C.G. Allred, G.M. Clark, R. Elledge, S.A.W. Fuqua, R.W. Brown, G.C. Chamness, C.K. Osborne and W.L. McGuire, Association of p53 protein expression with tumour cell proliferation rate and clinical outcome in node-negative breast cancer, *J. Natl. Cancer Inst.* **85** (1993), 200–206.

[2] M. Aubele, G. Auer, A. Voss, U. Falkmer, L.-E. Ruitquist and H. Höfler, Different risk groups in node negative breast cancer: Prognostic value of cytophotometrically assessed DNA, morphometry and texture, *Int. J. Cancer* **63** (1995), 7–12.

[3] G.U. Auer, R.G. Steinbeck and A.D. Zetterberg, Molecular markers in diagnostic pathology, Compendium on the Computerized Cytology and Histology Laboratory, 1994, 129–142.

[4] G.U. Auer, K.M. Heselmeyer, R.G. Steinbeck, E. Munck-Wikland and A.D. Zetterberg, The relationship between aneuploidy and p53 overexpression during genesis of colorectal carcinoma, *Virchows Arch.* **424** (1994), 343–347.

[5] H. Battifora, ed., p53 immunohistochemistry: A word of caution, *Hum. Pathol.* **25** (1994), 435–437.

[6] H.J.G. Bloom and W.W. Richardson, Histologic grading and prognosis in breast cancer, *Br. J. Cancer* **11** (1957), 359–377.

[7] C. Charpin, B. DeVictor, L. Andrac, J. Amabile, D. Bergert, M.-N. LaVaut, C. Allasia and L. Piana, p53 quantitative immunocytochemical analysis in breast cancer, *Hum. Pathol.* **26** (1995), 159–166.

[8] A.M. Davidoff, J.E. Herndon, N.S. Glover, B.-J.M. Kerns, J.C. Pence, J.D. Iglehart and J.R. Marks, Relation between p53 overexpression and established prognostic factors in breast cancer, *Surgery* **110** (1991), 259–264.

[9] U.G. Falkmer and S. Falkmer, The value of cytometric DNA analysis as a prognostic tool in neuroendocrine neoplastic diseases, *Path. Res. Pract.* **191** (1995), 251–303.

[10] U.G. Falkmer, A. Höög, H. Schimmelpfennig, O. Ahrens, G. Auer and S. Falkmer, A technique for cytometric DNA assessments of the nuclei of immunohistochemially identified neuroendocrine parenchymal cells, *Cytometry* **12** (1991), 26.

[11] K. Friedrich, V. Dimmer, G. Haroske, A. Loßnitzer, M. Kasper, F. Theissig and K.D. Kunze, Expression of p53 and bcl-2 in correlation to clinicopathological parameters, hormone receptor status and DNA ploidy in breast cancers, *Path. Res. Pract.* **191** (1995), 1114–1121.

[12] K. Friedrich, B. Thieme, G. Haroske, W. Meyer, V. Dimmer, F. Theissig and K.D. Kunze, Nuclear image analysis of p53 positive and p53 negative cells in breast carcinomas, *Anal. Quant. Cytol. Histol.* (in press).

[13] K. Friedrich, V. Dimmer, G. Haroske, W. Meyer, F. Theissig, B. Thieme and K.D. Kunze, Morphological heterogeneity of p53 positive and p53 negative nuclei in breast cancers stratified by clinicopathological variables, *Anal. Cell. Pathol.* (in press).

[14] W. Gorczyca, M. Markiewski, A. Kram, T. Tuziak and W. Domagala, Immunohistochemical analysis of bcl-2 and p53 expression in breast carcinomas: their correlation with Ki-67 growth fraction, *Virchows Arch.* **426** (1995), 229–233.

[15] G. Haroske, V. Dimmer, K. Friedrich, W. Meyer, B. Thieme, F. Theissig and K.D. Kunze, Nuclear image analysis of immunohistochemically stained cells in breast carcinomas, *Histochem. Cell Biol.* **105** (1996), 479–485.

[16] G. Haroske, K. Friedrich, F. Theissig, W. Meyer and K.D. Kunze, Heterogeneity of the chromatin fine structure in DNA-diploid breast cancer cells, *Anal. Cell. Pathol.* **8** (1995), 213–226.

[17] G. Haroske, W.D. Meyer, F. Theissig and K.D. Kunze, Increase of precision and accuracy of DNA cytometry by correcting diffraction and glare errors, *Anal. Cell. Pathol.* **9** (1994), 1–12.

[18] T. Illmer, unpublished study.

[19] *International Histological Classification of Tumours, Histological Typing of Breast Tumours*, 2nd edn, WHO, Geneva, 1981.

[20] M.B. Kastan, O. Onyekwere, D. Sidransky, B. Vogelstein and R.W. Craig, Participation of p53 protein in the cellular response to DNA damage, *Cancer Res.* **51** (1991), 6304–6311.

[21] K.D. Kunze, G. Haroske, V. Dimmer, W. Meyer and F. Theissig, Grading and prognosis of ductale mammary carcinoma by nuclear image analysis in tissue sections, *Path. Res. Pract.* **185** (1989), 689–693.

[22] D.P. Lane, p53, guardian of the genome, *Nature* **358** (1992), 15–16.

[23] A.J. Levine, J. Momand and C.A. Finlay, The p53 tumour suppressor gene, *Nature* **351** (1991), 453–456.

[24] G.M. Mariuzzi, V. Mambelli, P. Criante and S. Sisti, Quantitative evaluation of morphological parameters for infiltrating ductal breast cancer prognosis, *Path. Res. Pract.* **185** (1989), 698–700.

[25] L. Quiao, W. Peihong, A.H. Ghaleb, J.G. Pizzolo, T.B. Miller and M.R. Melamed, Bivariate flow cytometric analysis of p53 and DNA content in hepatocellular carcinoma, *Anal. Quant. Cytol. Histol.* **16** (1994), 124–130.

[26] W. Remmele and H.E. Stegner, Vorschlag zur einheitlichen Definition eines immunreaktiven Score (IRS) für den immunohistochemischen Estrogenrezeptor-Nachweis (ER-IRA) im Mammakarzinomgewebe, *Pathologe* **8** (1987), 138–140.

[27] Y. Remvikos, P. Laurent-Puig, R.J. Salmon, G. Frelat, B. Dutrillaux and G. Thomas, Simultaneous monitoring of p53 protein and DNA content of colorectal adenocarcinomas by flow cytometry, *Int. J. Cancer* **45** (1990), 450–456.

[28] R. Silvestrini, E. Benini, M.G. Daidone, S. Veneroni, P. Borachi, V. Cappelletti, G. di Fronzo and U. Veronesi, p53 as an independent prognostic marker in lymph node-negative breast cancer patients, *J. Natl. Cancer Inst.* **85** (1993), 965–970.

[29] B. Stenkvist, E. Bengtsson, O. Erikson, T. Jarkrans and B. Nordin, Image cytometry in malignancy grading of breast cancer. Results in a prospective study with seven years of follow-up, *Anal. Quant. Cytol. Histol.* **4** (1986), 293–300.

[30] F. Theissig, V. Dimmer, G. Haroske, K.D. Kunze and W. Meyer, Use of nuclear image cytometry, histopathological grading and DNA cytometry to make breast cancer prognosis more objective, *Anal. Cell. Pathol.* **3** (1991), 351–360.

[31] B. Vojtesek, J. Bartek, C.A. Midgley and D.P. Lane, An immunochemical analysis of the human nuclear phosphoprotein p53. New monoclonal antibodies and epitope mapping using recombinant p53, *J. Immunol. Meth.* **151** (1992), 237–244.